Available online at www.sciencedirect.com

SciVerse ScienceDirect

Ceramics International 38 (2012) 3291–3300

CERAMICS INTERNATIONAL

www.elsevier.com/locate/ceramint

Effect of NiO addition on properties of bulk yttria-doped ceria sintered from their spray pyrolyzed powder

Chin-Yi Chen *, Yang-Ru Lyu

Department of Materials Science and Engineering, Feng Chia University, No. 100, Wenhwa Rd., Seatwen, Taichung, 407, Taiwan

Received 29 November 2011; received in revised form 12 December 2011; accepted 13 December 2011
Available online 30 December 2011

Abstract

Since a nickel-containing anode (Ni content of generally >40 vol%) and electrolytes are commonly co-fired at high temperature (>1200 °C) in solid oxide fuel cell (SOFC) manufacturing, if Ni diffuses toward the electrolyte, the effects of the NiO on the properties of the electrolyte become relatively important. In the present study, nickel was added directly into the electrolyte ceramic, 10 mol% yttria-doped ceria (10YDC), during powder preparation to investigate the effects of the presence of NiO on the related properties of YDC electrolyte. 10YDC ceramics were sintered from spray pyrolyzed powders with various amounts of nickel addition (≤15 at%). The phase of the resulting powders was identified as a mixture of YDC and NiO after calcination in air. The grain size of as-pyrolyzed YDC particles decreased as NiO addition increased; however, the grain size of sintered YDC composite was increased by a small addition of NiO. NiO is believed to dissolve in YDC at high temperature, but it exhibits negligible solubility at room temperature. The excess NiO tended to segregate at the grain boundaries and thereby retard the grain growth in YDC matrices. The ac impedance data revealed that the precipitated NiO may reduce the conduction activation energy of the YDC electrolyte, increasing the conductivity of the YDC composite.

Keywords: A. Powders: chemical preparation; A. Sintering; B. Grain size; C. Electrical properties; D. CeO_2; E. Electrodes

1. Introduction

The solid oxide fuel cell (SOFC), which offers efficient power generation with low emission of pollutants, is one of the most promising electric power conversion systems. However, the high operating temperature and durability of SOFC materials raise the cost of development and limit practical application, so reducing the cost and lowering the operating temperature are important issues in the development of the SOFC system [1]. Thus, intermediate-temperature solid oxide fuel cells (IT-SOFC) have recently been receiving considerable attention due to the improved cost performance [2].

In recent years, research and development on IT-SOFC electrolytes have discovered that doped ceria-based solid electrolytes such as YDC (yttria-doped ceria) [3,4], SDC (samarium-doped ceria) [2,5,6] and GDC (gadolinium-doped ceria) [7–10] can be used as the electrolyte materials to replace YSZ (yttria-stablized zirconia), a high-temperature electrolyte, due to their high ionic conductivity in an intermediate temperature range (400–700 °C). However, in the operating temperature range and long-term operation, the anode materials, mainly consisting of a metal and an oxygen-conductive electrolyte, such as so-called cermet, may suffer metallic diffusion from the anode, which can affect the related properties of the solid electrolyte.

Nickel is commonly used as a metal component due to its high electronic conductivity, excellent hydrogen oxidation-catalytic properties, and high cost-effectiveness. During co-firing of anode supported and/or electrolyte supported fuel cells at a temperature higher than 1200 °C, the added nickel may vaporize, resulting in the loss of the nickel content in the ceramic composite. The metallic diffusion of Ni into the electrolyte materials is thus of crucial importance in such a process. Ou et al. [6] have estimated that the depth of Ni diffusion in the SDC electrolyte may be ~1 μm after co-sintering at 1400 °C for 25 h. The content of Ni in electrolyte has been estimated to be up to 18–22 at% near the anode/electrolyte interfaces. Although the Ni in the SOFC anode is

* Corresponding author. Tel.: +886 4 24517250x5313; fax: +886 4 24510014.
E-mail address: chencyi@fcu.edu.tw (C.-Y. Chen).

0272-8842/$36.00
doi:10.1016/j.ceramint.2011.12.036

generally around 40 vol% (~62.9 at% for Ni in 10YDC for a comparison with the present study) to ensure sufficient electrical conduction and catalytic properties [2], to the best of our knowledge, the effect of a small amount of diffused Ni content on the properties of the electrolyte material has not been clearly determined.

At intermediate temperatures, YDC may not have the highest ionic conductivity of all the doped ceria electrolytes, but it is the least costly. Thus, YDC is a promising replacement for the high-temperature electrolyte YSZ as the electrolyte material in SOFCs [11,12]. Various processes have been used to prepare doped ceria electrolytes, such as conventional solid-state ball milling [13–15], co-precipitation [5,11,16], sputter deposition [3], chemical vapor deposition (CVD) [4,17], sol–gel [18,19], and spray pyrolysis [2,8,10,20–22]. Spray pyrolysis (SP) has been widely utilized to synthesize nanocrystalline powders because it is a continuous process conducted under ambient pressure. Such a process is more economical than other processes, which involve numerous complex steps or must be performed under vacuum. Moreover, SP offers considerable possibilities for controlled synthesis of advanced ceramic powders and films due to its chemical adaptability [23].

Although many studies have used SP to prepare anode (cermet) and/or electrolyte for SOFC applications, most of them have stacked the anode/electrolyte together to form a ''cell stack'' for investigations of SOFC performance. As a result, the plain effects of diffused Ni in the electrolyte, as well as the use of pyrolyzed powders, have not been studied yet. Ni diffusion in electrolyte during operation of the SOFC has been reported by Ou et al. [6]. The methodology is to add Ni directly into the YDC ceramic, assuming that the Ni has diffused and exists within the YDC electrolyte. In the present study, Ni-doped YDC was prepared by SP from acetate based precursors. The effects of the Ni on the related properties of YDC are thus investigated.

2. Experimental procedures

To investigate the effect of Ni on the properties of YDC electrolyte, Ni was directly added into the YDC ceramics during powder preparation. 10 mol% yttria-doped ceria (10YDC) powders with and without Ni additions were homogeneously prepared using a bench-scale spray pyrolysis/electrostatic deposition (SP/ESD) system. The laboratory scale SP system consisted of a droplet generator, a homemade three-zone furnace, and a high-voltage cylindrical electrostatic collector. Precursor droplets were generated by a conventional ultrasonic nebulizer (King Ultrasonics Co., Ltd., Taiwan) with a resonant frequency of 1.65 MHz. The reaction temperature in the middle zone was set at 650 °C for powder formation. Details of the experimental set-up are described elsewhere [24,25]. The reaction temperature was determined by data from thermogravimetric analysis (TGA, Pyris 1 TGA, Perkin Elmer Co., USA) for the as-received precursors. The TGA was carried out under flowing air for removal of the product gases, with a heating rate of 40 °C/min. The precursors used for generation of 10YDC powder were CeA (cerium acetate) and YAH (yttria acetate hydrate) in an Y_2O_3/CeO_2 molar ratio of 10/90. The chemical formulas of CeA and YAH are $Ce(C_2H_3O_2)_3{\cdot}1.5H_2O$ (99.9%, Alfa Aesar, A Johnson Matthey Co.) and $(CH_3CO_2)_3Y{\cdot}xH_2O$ (Aldrich Chem. Co., Inc), respectively, and the chemicals used were reagent grade, with >99% purity. Nickel acetate hydrate (NiAH) was used as the precursor for the additions of NiO. The chemical formula of NiAH is $Ni(C_2H_3O_2)_2{\cdot}4H_2O$ (Showa Chem. Co., Ltd.). The respective molecular weights of CeA, YAH, and NiAH reported by the manufacturers are 344, 266, and 249. The concentrations of precursor solutions, (CeA + YAH) or (CeA + YAH + NiAH) in de-ionized water, were both 1.0 wt% for atomization.

To further remove the residual organics and confirm the formation of the oxides in the resulting powders, the as-pyrolyzed powders were calcined at a temperature of 950 °C for 5 h in air (TF55035A, Lindberg/Blue M, USA). The heating and cooling rates were 5 °C/min. The powder was formed into disks 8 mm in diameter and ~1.5 mm thick by uniaxial pressing at 60 MPa; no binder was used in the present study. These compacts were buried in pure ZrO_2 powder and sintered in a covered alumina (Al_2O_3) crucible at 1600 °C for 10 h in air (BF51314C, Lindberg/Blue M, USA) without any sintering aid. The heating and cooling rates were both 5 °C/min. The crystallites in as-pyrolyzed particles were observed using high-resolution transmission electron microscopy (HRTEM, JEOL 3000F, Japan). The morphology of as-pyrolyzed powders and sintered compacts was observed using field emission scanning electron microscopy (FE-SEM, JSM-6700F, JEOL, Japan). The phase identification was examined using X-ray diffractometry (XRD, D8 SSS, Bruker, German).

A lighter-colored surface layer was observed on the Ni-containing specimens after sintering. The vapor pressure of NiO is high at temperatures near its melting point (1955 °C) [26], and this high pressure resulted in a thin, Ni-depleted surface layer after sintering. This was corroborated by the observation of a green NiO-coated layer on the covered ZrO_2 powder and the inner surfaces of the crucible. Both surface layers of the sintered disks were removed by grinding with SiC sandpaper before any measurements were taken. Since the specimens were buried in a pure ZrO_2 powder bed during sintering, this procedure also removed the ZrO_2 diffusion layer. The final density was determined using the Archimedes method. The solubility of NiO in 10YDC can be assumed to be negligible (as will be demonstrated later); therefore, the theoretical density of the NiO-added 10YDC was estimated using values of 7.01 g/cm^3 for 10YDC and 6.67 g/cm^3 for NiO. The polished surfaces were prepared by grinding with SiC particles and polishing with 0.3 μm α-Al_2O_3 particles. The grain boundaries and microstructures were revealed by thermal etching of the composites at 1470 °C for 30 min. The microstructure was observed via scanning electron microscopy (SEM). The amount of Ni within the 10YDC grains was determined using electron probe microanalysis (EPMA, JXA-8200, JEOL Co., Tokyo, Japan) before thermal etching at an accelerated voltage of 30 KeV. An undoped 10YDC specimen, prepared using the same procedures, was used as the reference specimen.

The sintered specimens for electrical property measurements were polished, and both surfaces of the disk specimens were screen-painted with a platinum (Pt) paste. Two flat-pressed Pt wires with a diameter of 0.5 mm (thermocouple grade) were attached to the Pt paste. The as-pasted specimens with Pt wires were heated to 1000 °C for 20 min in air for the Pt electrode sintering. The electrical properties of the 10YDC specimens with and without Ni addition were examined using ac impedance spectroscopy (Hioki 3532-50 LCR Hitester, Japan) within a frequency domain of 42 Hz to 5 MHz, an ac amplitude of 50 mV, and 50 mV bias. The impedance spectra were recorded in a tubular furnace at a temperature range of 400–700 °C under ambient atmosphere. The total electrical conductivity of the specimens was estimated from the impedance spectra using the impedance analysis software provided by the instrument manufacturer (ZView, 2nd ed., Scribner Associates Inc., Southern Pines, NC) for equivalent circuit analysis.

3. Results and discussion

In the beginning of the present study, the weight losses of the as-received precursors during heating were confirmed by their TGA data, as shown in Fig. 1. Curve (a) shows that CeA experienced three major weight loss mechanisms in the temperature ranges of 100–200 °C, 300–420 °C, and 420–680 °C. Based on the molecular weights of CeA and its decomposition products, the first and the last loss mechanisms are attributable to dehydration and conversion into CeO_2, respectively. The middle weight loss mechanism is attributed to decomposition of CeA to acetic acid and cerium hydroxide ($Ce(OH)_3$) [27]. Curve (b) shows that the YAH was dehydrated and converted into yttrium hydroxide at a temperature below 430 °C, after which it converted into yttrium oxide in the temperature range of 430–630 °C. Moreover, the NiAH, curve (c), finished its conversion into nickel oxide at a temperature below 480 °C. These results suggest that the reaction temperature of these precursors should be set at a temperature

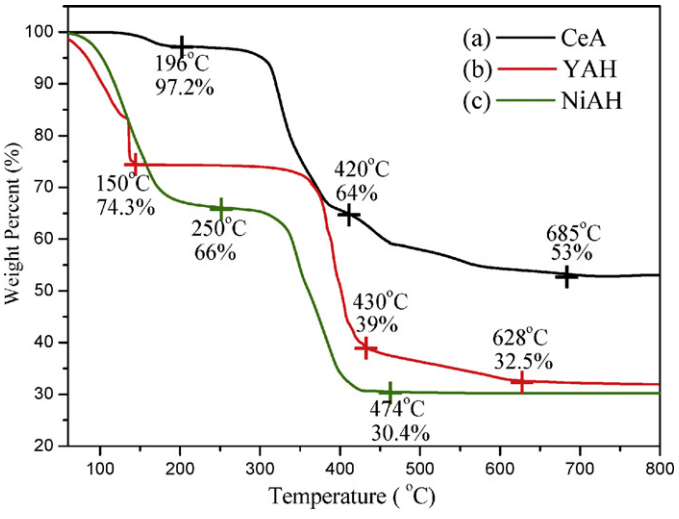

Fig. 1. Thermogravimetric analysis (TGA) curves of precursors (a) CeA, (b) YAH, and (c) NiAH.

higher than 650 °C to ensure that the primary oxidization reaction of the precursors occurs during SP.

Fig. 2 shows the SEM micrographs of the SP resulting powders obtained at the reaction temperature of 650 °C with increases in the NiO content. The YDC particles were spherical and had uneven surfaces. Due to the broad drop size distribution generated by the 1.65 MHz nebulizer, based on the theory of the one-particle-per-drop mechanism [23], the size of the YDC particles ranged from 80 nm to hundreds of nanometers. It can be noticed that the particle size first increased with the increase in NiO content, and it subsequently decreased when 15 at% NiO was added. The YDC particles tended to form a hollow structure due to the surface precipitation of the precursor CeA during SP [23,27]. The shriveled surfaces of the particles may have resulted from shrinkage during cooling, when the hollow particles travelled out of the tubular reactor. The shrinkage of the SP particles was more severe with increases in NiO content. This suggests that the inhomogeneous distribution of the added NiO in the YDC particles resulted in different shrinkage rates on the surface of the particle shell during cooling. Such a particle structure may have influenced the following consolidation of the NiO-added YDC green compacts.

To confirm the product phase of the SP powders before and after calcination, as well as their crystallinities, X-ray diffractometry was carried out as a function of NiO content in ambient conditions, as shown in Fig. 3. Fig. 3(a) shows the XRD patterns of the as-pyrolyzed YDC powders containing various amounts of NiO. The SP powders were identified as a phase of yttria-doped ceria with a fluorite structure. No significant differences in phase identification were revealed for YDC powders when the NiO content was increased. However, it should be noted that the widths of the diffraction peaks broadened with increases in NiO addition. This broadening suggests that the crystallinity of the SP YDC powders was inhibited by NiO addition. The size of the nanocrystallite was estimated by Scherrer's formula to range from 1.4 to 1.9 nm, showing a trend of decreases with increased NiO content (to be shown in Fig. 6). The crystallite size was confirmed by TEM observation. Fig. 4 shows the HRTEM micrographs of the as-pyrolyzed YDC particle with and without NiO addition. Note that the SP particle was nanometer-sized and polycrystalline in structure. Amorphous and nanocrystalline structures are commonly observed in SP powders. The nanosized grains may be attributed to the relatively short residence time (~5 s) of the precursor drops during SP, which did not allow much time for the generated grains in the YDC particles to coalesce. That is, each resulting CeO_2 particle contained many extremely small crystallites after SP. The crystallites are denoted with irregular open polygons in the HRTEM images. As seen in the micrographs, the crystallite of NiO-added YDC was slightly smaller than that of the unadded one. The addition of NiAH precursor may prolong the crystallite formation of YDC in the particle during SP. Moreover, residual organics were believed to exist in the SP powders and may have inhibited the crystallization of YDC. Fig. 3(b) shows the XRD patterns of the heat-treated YDC powders as a function of NiO addition. The sharp diffraction peaks suggest that the heat-treated powders

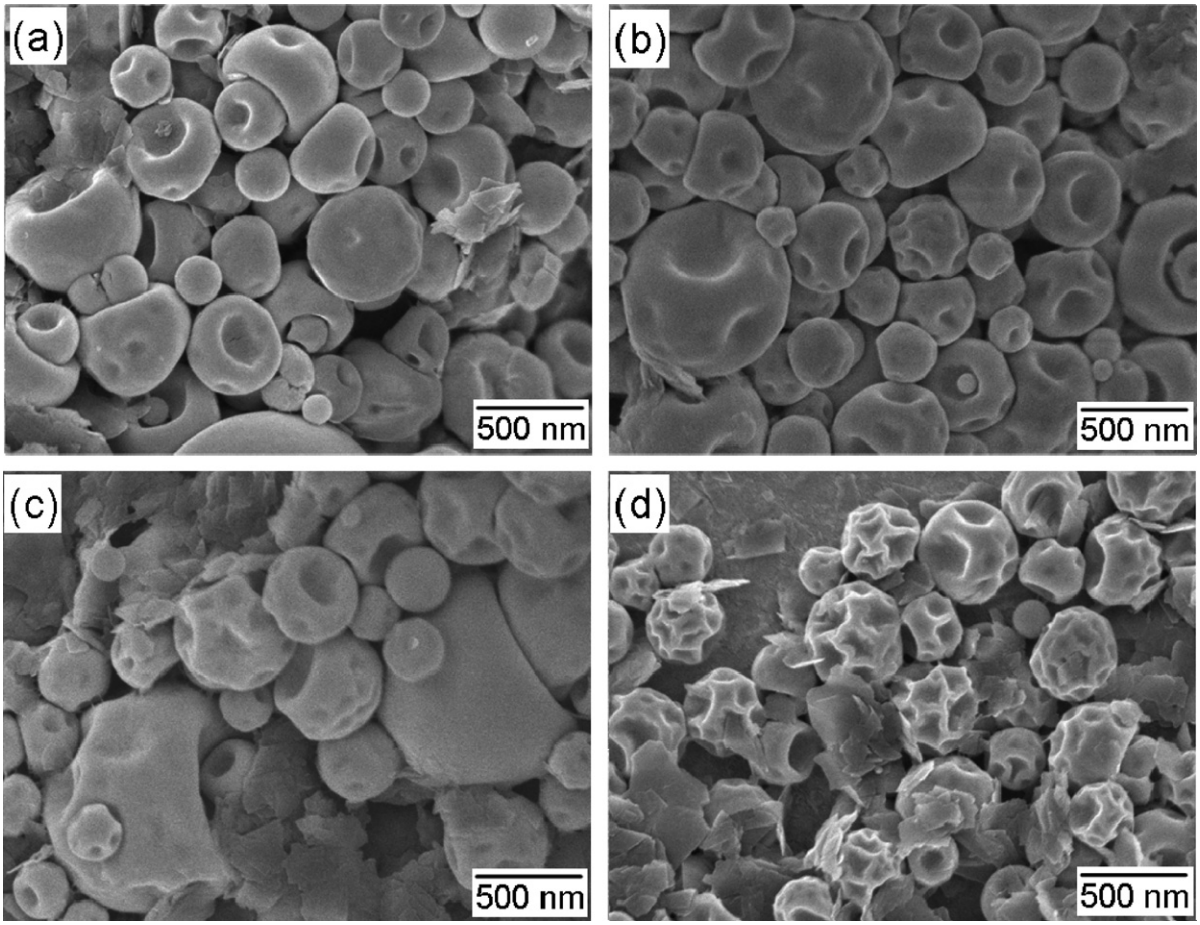

Fig. 2. FESEM micrographs of SP powders obtained at a reaction temperature of 650 °C: (a) 10YDC, (b) $(10YDC)_{95}(NiO)_5$, (c) $(10YDC)_{90}(NiO)_{10}$, (d) $(10YDC)_{85}(NiO)_{15}$.

were well-crystallized, identifying them as a phase of YDC with a fluorite structure. Diffraction peaks of NiO are indicated for the powders containing 10 and 15 at% NiO contents, while those for 5 at% NiO are not obvious due to its low amount of addition.

The heat-treated powders were formed into discs by uniaxial pressing for follow-up sintering processes. Fig. 5 shows the SEM micrographs of the sintered YDC bulks with various amounts of NiO addition. The grain size increased when 5 at% NiO was added, and then decreased with further increases in NiO content. Fig. 6 shows the grain sizes of the respective as-pyrolyzed YDC powders and the sintered bulks derived from the corresponding SP powders as a function of NiO content. The effect of NiO addition on the crystallite size of the as-pyrolyzed powder has been discussed earlier. It can be seen in Fig. 6 that the grain size of the sintered YDC bulk ranged from 5 μm to 20 μm and reached its highest value when a small amount of NiO was added. This phenomenon is generally thought to be due to the presence of a phase in a volatile state or the dissolution of an additive in the matrix during sintering [28]. The distribution of NiO may not be uniform when the amount of NiO is small. Such heterogeneity, including partial dissolution of the additive (if dissolution occurred in this system at high temperature), may have triggered the grain growth during sintering. NiO is volatile during sintering at 1600 °C (the melting point of bulk NiO is 1955 °C), so it may have dragged the nearby grains close together during the vaporization process. Grains preferentially coalesce with their adjacent grains when the NiO drains in the grain contacts. The grain growth was thus significant when a small amount of NiO was added.

With increased amounts of NiO added, a uniform distribution of the NiO phase in YDC would be obtained more easily. The inhibition of grain growth tended to start when there was excess NiO on YDC grain boundaries. Fig. 7 shows the SEM micrographs of YDC doped with 10 at% NiO after appropriate thermal etching, imaged by secondary electrons (SE) and back-scattered electrons (BSE), respectively. The BSE image gives more specific information on the distribution of the phases present than does the SE image. As seen in both micrographs, a secondary phase can be noticed at the grain boundaries in the YDC ceramics. Although NiO is probably dissoluble in YDC at high temperature [29], the solubility of NiO in YDC has been reported to be improbable at room temperature [30,31]. Recalling the grain size data in Fig. 6, the largest grain size of the sintered bulk with 5 at% NiO also suggested that the formation of solid solution occurred at high temperature. The aliovalent cation addition may induce a

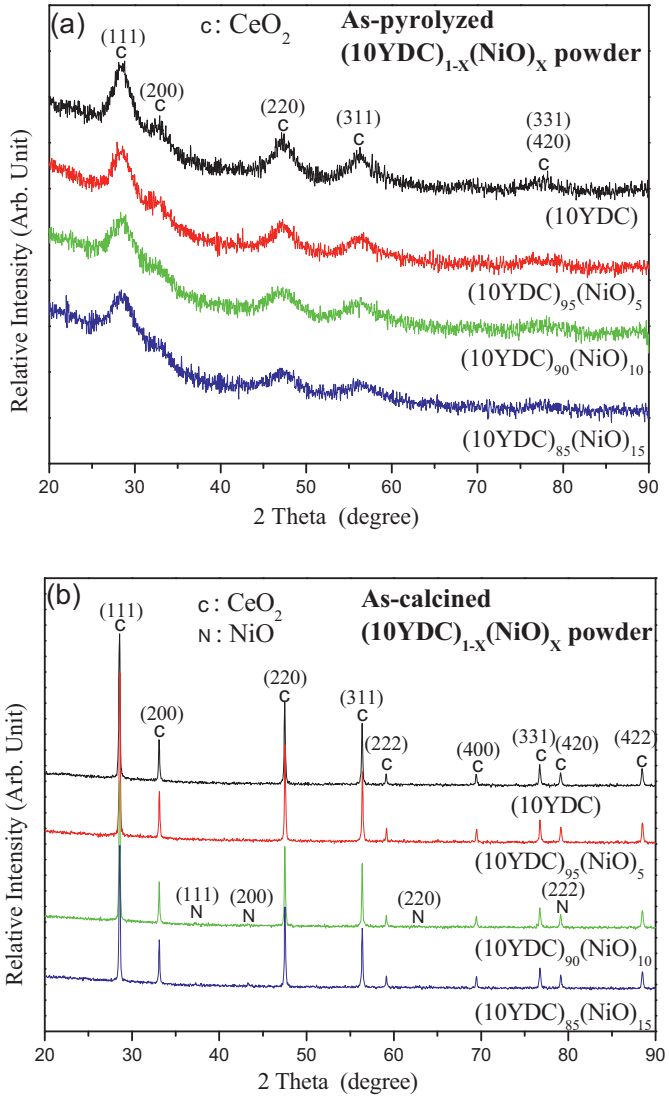

Fig. 3. XRD patterns of (a) as-pyrolyzed and (b) as-calcined 10YDC powders as a function of NiO content. The SP and calcination temperatures were 650 °C and 950 °C, respectively.

higher concentration of defects in the host lattice, resulting in the grain coalescence of the NiO/YDC composite. However, the excess NiO tended to segregate at the grain boundaries of the YDC during the cooling process, thereby inhibiting the grain size of the composite. Fig. 8 shows the typical EPMA measurement results for the sintered YDC bulk with 10 at% NiO. EPMA is known to be a powerful tool in electron microprobe analysis to quantify chemical compositions with high accuracy and to detect rather low concentrations, even for light elements. Because the electron penetration depth, as detected by the microprobe, was estimated to be <4.5 μm at an accelerated voltage of 30 KeV, the line scan data between the secondary phase, with a distance of ∼18 μm according to EPMA measurement, can be regarded as appropriate and effective. The EPMA data shows the secondary inclusions to be a Ni-containing phase. The data also indicate that the Ni content between both inclusions was approximately zero, suggesting that the dissolution of NiO in YDC was negligible at room temperature when the composites were sintered in air. Though the volatile NiO near the bulk surface may vaporize, such interior non-miscible NiO phase on grain boundaries can play a role in retarding the grain growth of YDC electrolyte during sintering, as seen in Fig. 7. A similar phenomenon, known as the pinning effect, has also been reported in a NiO/GDC system [7]. Furthermore, the presence of intragranular pores can be thought to show little inhibition of the grain growth in ceramic bulks. The influence of the segregated NiO on grain growth of the YDC bulk is thus suggested to predominate in this system.

In the sintered microstructures, shown in Fig. 5, the porosity tended to increase with greater additions of NiO. Both intergranular and intragranular pores can be observed in these micrographs. In other words, the density of the sintered bulk appears to have decreased when NiO was present. Fig. 9 shows the relative densities of the sintered YDC bulks as a function of NiO addition. The decline in density with increasing NiO addition shows good agreement with the results of the micrographs in Fig. 5. The hollow structure and increasingly

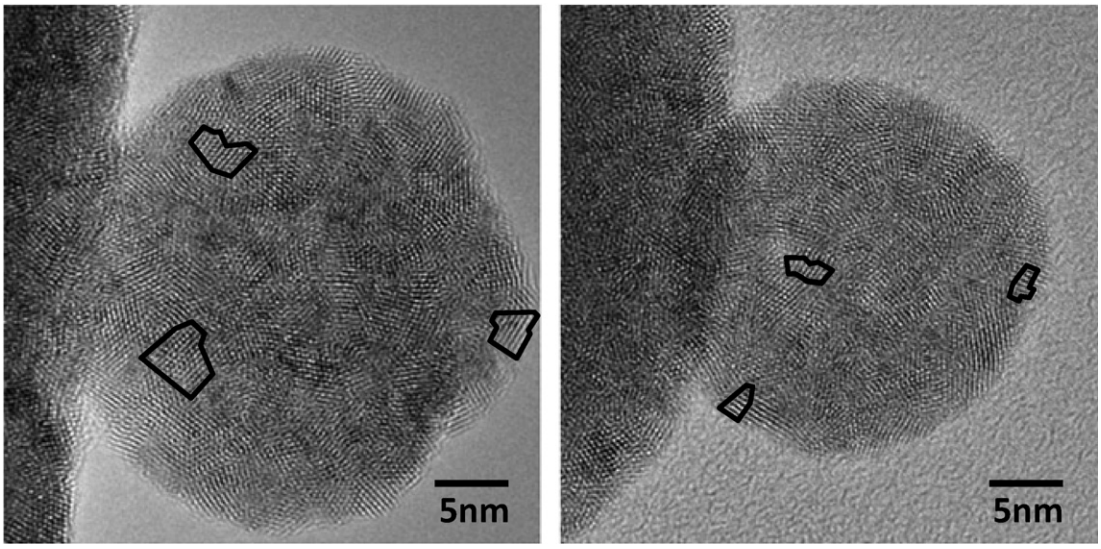

Fig. 4. HRTEM micrographs of SP powders obtained at a reaction temperature of 650 °C: (a) 10YDC, (b) $(10YDC)_{85}(NiO)_{15}$.

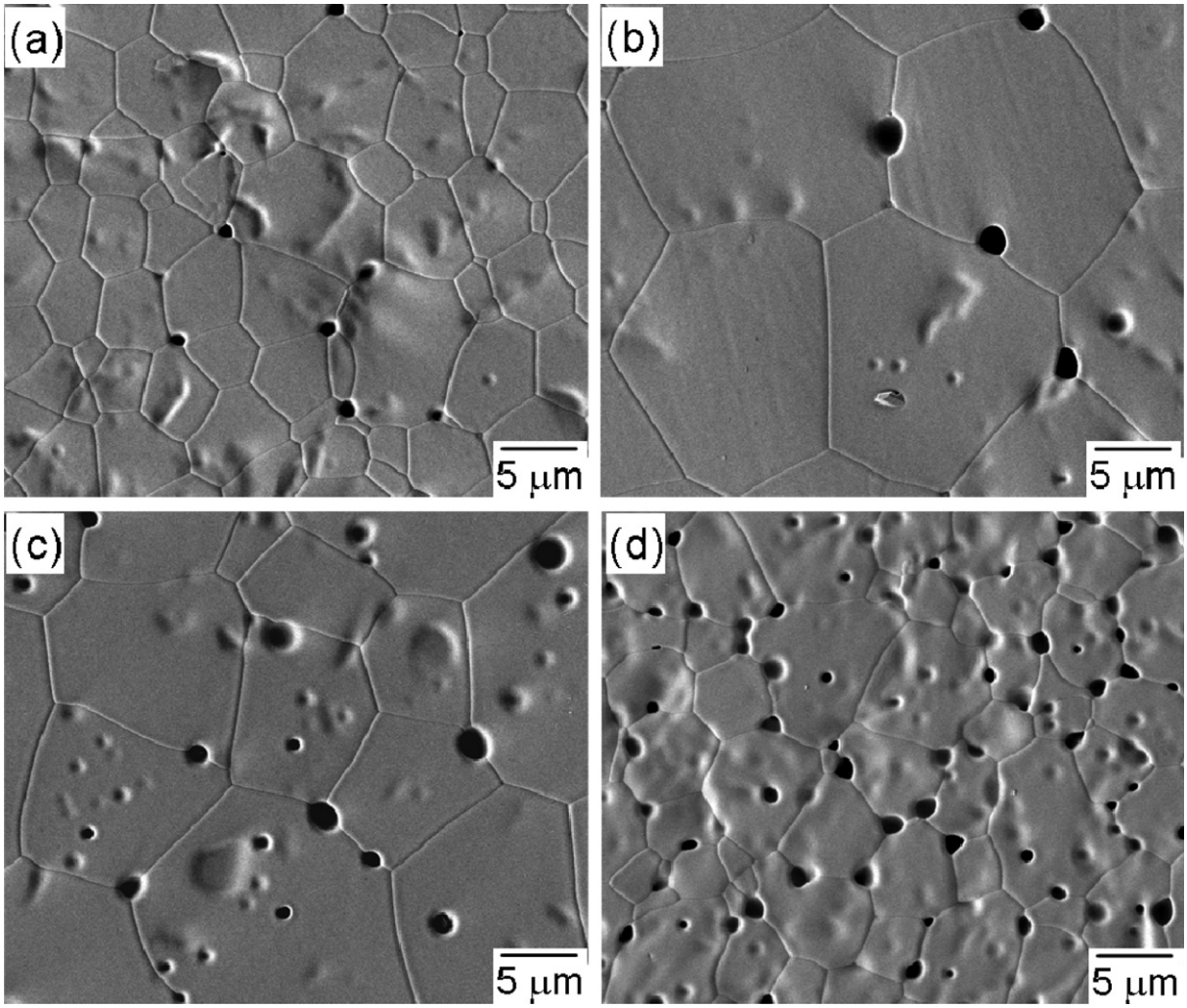

Fig. 5. FESEM micrographs of sintered (a) 10YDC, (b) $(10YDC)_{95}(NiO)_5$, (c) $(10YDC)_{90}(NiO)_{10}$, and (d) $(10YDC)_{85}(NiO)_{15}$. Specimens were sintered at 1600 °C for 10 h in air.

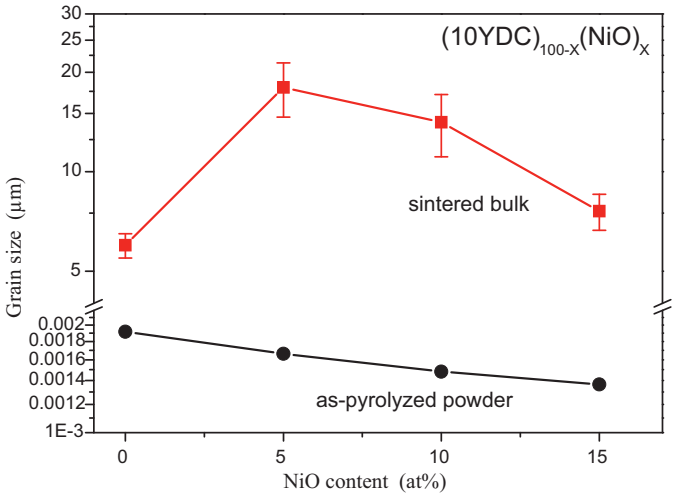

Fig. 6. Grain size of as-pyrolyzed 10YDC powder and its sintered bulk as a function of NiO content.

uneven surfaces of the particles obtained from SP, shown in Fig. 2, may have caused the decline in sintered density. However, the relative densities ranged from 99.8% to 94.5%, revealing values comparable to those reported in the literature [11,32,33]. Ceria-based ceramics have been reported by many researchers to be difficult to densify, even at an elevated temperature of 1600 °C. A typical density of 95% relative to theoretical at sintering temperatures of 1550–1600 °C has been obtained. Therefore, the relative density of the sintered YDC is believed to be relatively high as compared to those in the literature. A structure without interconnected pores or channels under such a relative density is still capable of meeting the requirements of solid electrolyte in SOFC.

To investigate the influence of the NiO that segregated in the YDC grain boundary region, ac impedance spectroscopy was carried out to estimate the grain-boundary electrical conductivity of YDC as a function of NiO content at various temperatures. Figs. 10 and 11 show the impedance diagrams of,

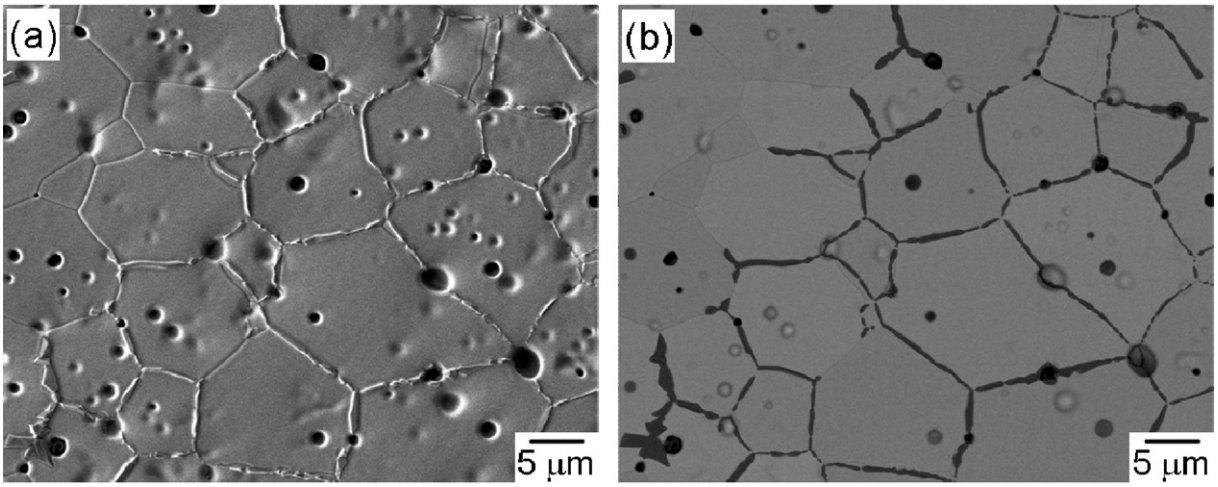

Fig. 7. FESEM micrographs of sintered $(10YDC)_{90}(NiO)_{10}$ bulk imaged by (a) secondary electrons and (b) back-scattered electrons.

respectively, the undoped YDC and that doped with 15 at% NiO as a function of temperature (the results for specimens with 5 at% and 10 at% NiO are not shown here). Measurements were carried out in air. The lower-right insets in both diagrams show the details of the higher-frequency regions. Such impedance data can be expected to provide respective conductivities contributed by the grain interior and grain boundary in ceramic bulks. Moreover, the inset in the upper-left corner of Fig. 10 is a schematic drawing of an idealized impedance spectrum associated with an equivalent circuit model simulated and fitted using a nonlinear least-squares fitting program for the spectrum recorded at lower temperature. The fitting results are similar to those demonstrated by Zając and Molenda [34].

In both figures, Figs. 10 and 11, imperfect semi-circles and diffusion tails (on the extreme right, appearing at the low frequency end of the diagrams) can be observed for both specimens with heating at 400 °C. The diffusion tail, which may be attributed to the electrode polarization response (charge transfer and diffusion processes occurred on the interface between specimen and Pt electrode), represents a parallel arrangement of a resistor R_{ct} and a constant phase element (CPE, instead of pure capacitance) in the equivalent circuit. The left side of the semi-circle, intercepting the real impedance axis (estimated with a data-fitting program), may give resistivity associated with the intragrain response (corresponding to the R_{gi} resistance in the equivalent circuit); in contrast, the other side of the semi-circle, intercepting the diffusion tail, may be assigned to the intergrain resistance (corresponding to R_{gb} element in the equivalent circuit). This shows that the conductivity data obtained from the impedance diagrams can separate the contribution of the grain, grain-boundary, and electrode polarization responses.

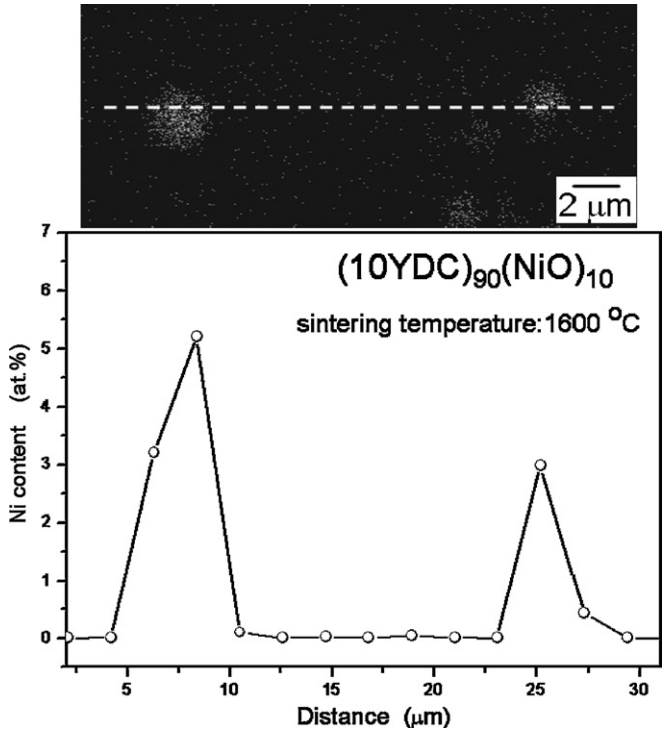

Fig. 8. Typical EPMA measurement results for the 10YDC doped with 10 at% Ni. The specimen was sintered at 1600 °C for 10 h in air.

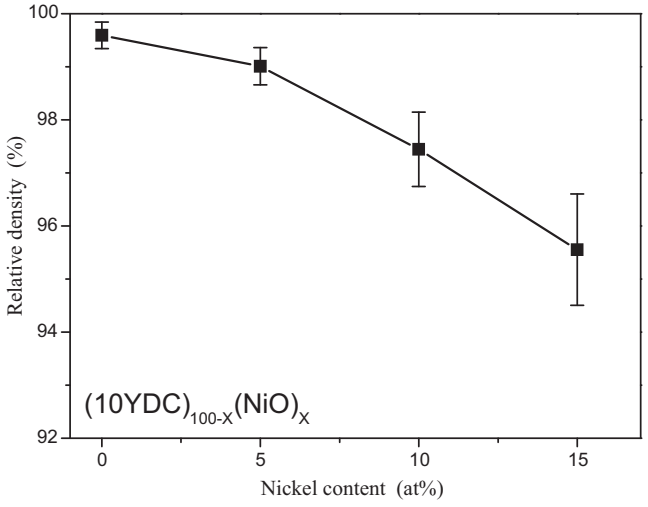

Fig. 9. Relative densities of the sintered 10YDC bulks as a function of NiO content.

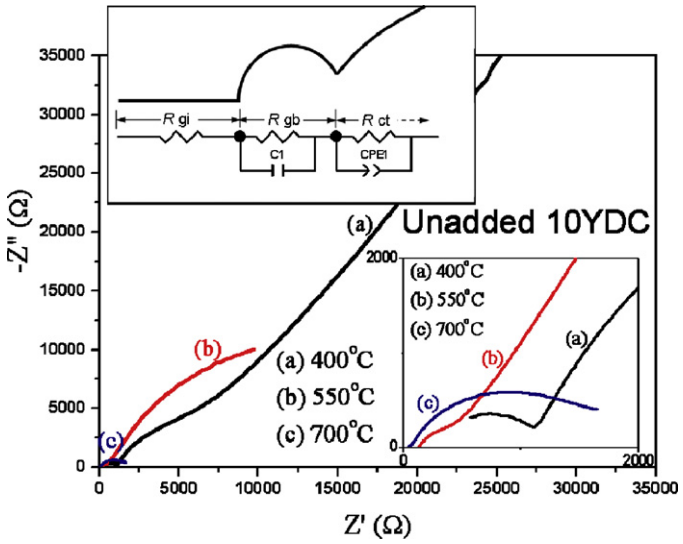

Fig. 10. Impedance plots of undoped 10YDC as a function of temperature. The upper-left and the lower-right insets show the schematic diagram of an idealized impedance spectrum associated with an equivalent circuit and the data obtained in the higher frequency range.

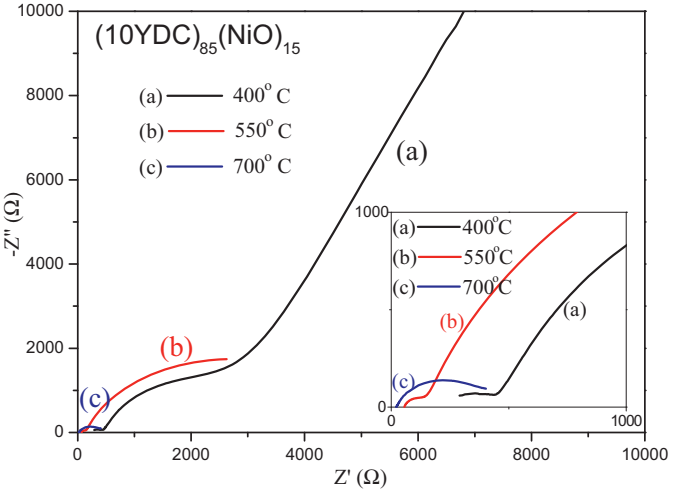

Fig. 11. Impedance plots of $(10YDC)_{85}(NiO)_{15}$ as a function of temperature. The inset shows the data obtained in the higher frequency range.

With an increase in heating temperature to 550 °C, the semi-circle shifts to the higher frequency, indicating an increase in the grain conductivity. The semi-circle and the diffusion tail cause an increase in degrees of overlap, suggesting that the electrode polarization dominates as the temperature rises, and the resistance contribution of the grain boundary was indistinct. The grain boundary resistance is thus revealed to be depressed at elevated temperature. With temperature further elevated to 700 °C, the grain-boundary semi-circle almost disappears entirely, and the electrode diffusion tail shifts further to the higher frequency, increasing its conductivity. It is not easy to distinguish the contribution of the grain-boundary resistance from that of the grain interior at such a high measurement temperature. Moreover, the activation energy calculated for total conductivity of the specimen is attributed to those of the grain interior and grain boundary ($R_{tot} = R_{gi} + R_{gb}$) [35]. These impedance spectra, recorded at different temperatures, were fitted with a same equivalent model; then the total conductivities contributed by the combination of grain interiors and grain boundaries of all specimens were analyzed and plotted as a function of the inverse heating temperature [34,36].

Because the electrical conductivity of YDC electrolyte is a thermally activated process, the temperature dependence of the conductivity behavior can be described by the Arrhenius equation,

$$\sigma T = \sigma_0 \exp\left(-\frac{E_a}{kT}\right) \quad (1)$$

where σ is the electrical conductivity, σ_0 is a constant that depends on the sample, E_a is the activation energy for conductivity, k is the Boltzmann constant, and T is the absolute temperature. Fig. 12 shows the Arrhenius plots for the electrical conductivities of 10YDC as various amounts of NiO were added. In that figure, the total conductivity of the YDC electrolyte increases with the increase in NiO content, and it also increases with elevated heating temperature. The increase in conductivity with increasing NiO content may result from the presence of NiO, a *p*-type oxide semiconductor, on the grain boundary of YDC electrolyte. As can be seen in this figure, the plots give four fitted straight lines over a temperature range of 550–700 °C, indicating that the total conductivities of the specimens followed the Arrhenius equation. The activation energies of total conductivities ($E_{a,tot}$) can thus be determined from the slopes of the lines, as indicated in Fig. 12. The activation energies for additions of 0, 5, 10, and 15 at% NiO to YDC electrolyte are 1.87, 1.65, 1.41 and 1.26 eV, respectively. The $E_{a,tot}$ of YDC decreases with the increase of NiO addition. Because the activation energy for total conductivity is close to the one related to the grain-boundary response [34], as shown in Fig. 7, the influence of NiO segregation between the YDC grains on the electrical properties becomes dominant in this system. Moreover, as shown in Fig. 6, a decrease in grain size may cause an increase in the area of grain boundaries when NiO is added. This effect may also become more significant with increases in the amount of NiO content.

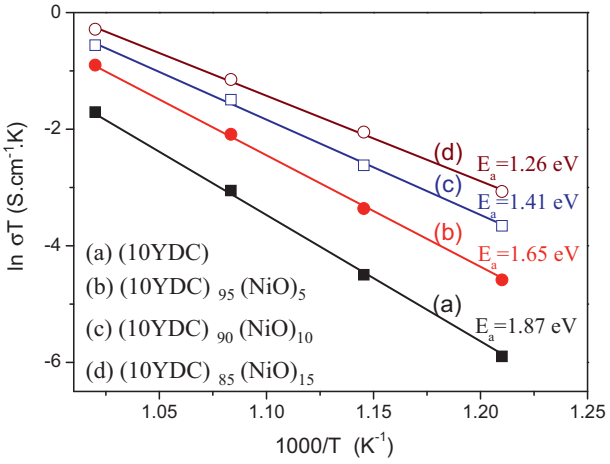

Fig. 12. Arrhenius plots for total conductivity of 10YDC as a function of NiO content.

For YDC electrolytes, the activation energies reported in the literature [4,11,34] generally range from ca. 0.66 to 0.86 eV. However, the activation energy of unadded 10YDC calculated in the present system shows a relatively high value. The conductivity of the YDC measured in this system is found to be much lower than that reported by Ou et al. [6]. Most likely, this is due to the presence of Ce^{3+} cations in the YDC lattice, pyrolyzed from the precursor CeA (Ce^{3+}) during SP. The intermediate phase, decomposed from CeA to CeO_2, was identified as $Ce(OH)_3$ by TGA (Fig. 1). A large number of Ce^{3+} ions are thus believed to have remained in the CeO_2 lattice. In addition, the heating of the specimens at a temperature higher than ca. 400 °C can induce the formation of Ce^{3+} ions in undoped ceria. These effects could be enhanced in highly doped ceria [37]. Moreover, Ou et al. [6] also pointed out that Ce^{3+} ions could cause an increase in the concentration and ordering of oxygen vacancies, thereby reducing the ionic conduction.

4. Conclusions

10YDC electrolytes with various amounts of NiO additions were successfully prepared from their SP powders in the present study. The influences of NiO on the properties of YDC electrolyte were investigated by directly adding Ni into the YDC powder during the powder preparation. The NiO tended to make the surfaces of the SP particles to significantly uneven, resulting in poor densification of the sintered YDC ceramics. Moreover, a small amount of NiO may enhance the grain growth of YDC during sintering; subsequently, the non-miscible NiO may segregate on the grain boundaries in the YDC matrix and thereby inhibit the grain growth of YDC electrolyte with increased amounts of NiO. With increased NiO addition, the conduction activation energy of YDC electrolyte was decreased, but the total conductivity was increased in this system.

Acknowledgements

The authors would like to thank the National Science Council of Taiwan for financially supporting this work under Grants No. NSC 99-2221-E-035-032-MY3 and NSC 100-2628-E-035-002. The authors also thank the FCU for partial financial support under a New Star Project.

References

[1] J.P.P. Huijsmans, F.P.F. Van Berkel, G.M. Christie, Intermediate temperature SOFC – a promise for the 21st century, J. Power Sources 71 (1998) 107–110.
[2] S. Suda, K. Kawahara, M. Kawano, H. Yoshida, T. Inagaki, Preparation of matrix-type nickel oxide/samarium-doped ceria composite particles by spray pyrolysis, J. Am. Ceram. Soc. 90 (2007) 1094–1100.
[3] T. Tsai, E. Perry, S. Barnett, Low-temperature solid-oxide fuel cells utilizing thin bilayer electrolytes, J. Electrochem. Soc. 144 (1997) L130–L132.
[4] H.B. Wang, H.Z. Song, C.R. Xia, D.K. Peng, G.Y. Meng, Aerosol-assisted MOCVD deposition of YDC thin films on (NiO + YDC) substrates, Mater. Res. Bull. 35 (2000) 2363–2370.
[5] X. Fang, G. Zhu, C. Xia, X. Liu, G. Meng, Synthesis and properties of Ni–SDC cermets for IT–SOFC anode by co-precipitation, Solid State Ionics 168 (2004) 31–36.
[6] D.R. Ou, T. Mori, F. Ye, M. Miyayama, S. Nakayama, J. Zou, G.J. Auchterlonie, J. Drennand, Microstructural characteristics of SDC electrolyte film supported by Ni–SDC cermet anode, J. Electrochem. Soc. 156 (2009) B825–B830.
[7] V. Gil, A. Larrea, R.I. Merino, V.M. Orera, Redox behaviour of Gd-doped ceria–nickel oxide composites, J. Power Sources 192 (2009) 180–184.
[8] L.D. Jadhav, M.G. Chourashiya, A.P. Jamale, A.U. Chavan, S.P. Patil, Synthesis and characterization of nano-crystalline $Ce_{1-x}G_{dx}O_{2-x/2}$ (x = 0–0.30) solid solutions, J. Alloys Compd. 506 (2010) 739–744.
[9] U.P. Muecke, S. Graf, U. Rhyner, L.J. Gauckler, Microstructure and electrical conductivity of nanocrystalline nickel- and nickel oxide/gadolinia-doped ceria thin films, Acta Mater. 56 (2008) 677–687.
[10] U.P. Muecke, K. Akiba, A. Infortuna, T. Salkus, N. Stus, L.J. Gauckler, Electrochemical performance of nanocrystalline nickel/gadolinia-doped ceria thin film anodes for solid oxide fuel cells, Solid State Ionics 178 (2008) 1762–1768.
[11] J. Van herle, T. Horita, T. Kawada, N. Sakai, H. Yokokawa, M. Dokiya, Fabrication and sintering of fine yttria-doped ceria powder, J. Am. Ceram. Soc. 80 (1997) 933–940.
[12] C.H. Cheng, S.F. Lee, C.W. Hong, Ionic dynamics of an intermediate-temperature yttria-doped-ceria electrolyte, J. Electrochem. Soc. 154 (2007) E158–E163.
[13] H. Yoshida, H. Deguchi, K. Miura, M. Horiuchi, T. Inagaki, Investigation of the relationship between the ionic conductivity and the local structures of singly and doubly doped ceria compounds using EXAFS measurement, Solid State Ionics 140 (2001) 191–199.
[14] Y. Xiong, K. Yamaji, T. Horita, N. Sakai, H. Yokokawa, Electronic conductivity of 20 mol% $YO_{1.5}$ doped CeO_2, J. Electrochem. Soc. 149 (2002) E450–E454.
[15] Q.L. Liu, K.A. Khor, S.H. Chan, X.J. Chen, Anode-supported solid oxide fuel cell with yttria-stabilized zirconia/gadolinia-doped ceria bilayer electrolyte prepared by wet ceramic co-sintering process, J. Power Sources 162 (2006) 1036–1042.
[16] J. Van herle, T. Horita, T. Kawada, N. Sakai, H. Yokokawa, M. Dokiya, Low temperature fabrication of (Y,Gd,Sm)-doped ceria electrolyte, Solid State Ionics 86–88 (1996) 1255–1258.
[17] M. Pan, G.Y. Meng, H.W. Xin, C.S. Chen, D.K. Peng, Y.S. Lin, Pure and doped CeO_2 thin films prepared by MOCVD process, Thin Solid Films 324 (1998) 89–93.
[18] W. Huang, P. Shuk, M. Greenblatt, Properties of sol–gel prepared $Ce_{1-x}Sm_xO_{2-x/2}$ solid electrolytes, Solid State Ionics 100 (1997) 23–27.
[19] X. Luo, B. Zhu, C. Xia, G.A. Niklasson, C.G. Granqvist, Transparent ion-conducting ceria-zirconia films made by sol–gel technology, Solar Energy Mater. Solar Cells 53 (1998) 341–347.
[20] D. Perednis, L.J. Gauckler, Solid oxide fuel cells with electrolytes prepared via spray pyrolysis, Solid State Ionics 166 (2004) 229–239.
[21] S. Suda, M. Itagaki, E. Node, S. Takahashi, M. Kawano, H. Yoshida, T. Inagaki, Preparation of SOFC anode composites by spray pyrolysis, J. Euro. Ceram. Soc. 26 (2006) 593–597.
[22] M. Kawano, H. Yoshida, K. Hashino, H. Ijichi, S. Suda, K. Kawahara, T. Inagaki, Synthesis of matrix-type NiO–SDC composite particles by spray pyrolysis with acid addition for development of SOFC cermet anode, J. Power Sources 173 (2007) 45–52.
[23] G.L. Messing, S.C. Zhang, G.V. Jayanthi, Ceramic powder synthesis by spray pyrolysis, J. Am. Ceram. Soc. 76 (1993) 2707–2726.
[24] C.Y. Chen, C.K. Lin, Y.R. Lyu, H.H. Lin, W.H. Tuan, Pseudocapacitive manganese oxide prepared by a spray pyrolysis/electrostatic deposition technique, Adv. Sci. Technol. 45 (2006) 1896–1901.
[25] C.-Y. Chen, Y.-R. Lyu, C.-Y. Su, H.-M. Lin, C.-K. Lin, Characterization of spray pyrolyzed manganese oxide powders deposited by electrophoretic deposition technique, Surf. Coat. Technol. 202 (2007) 1277–1281.
[26] O. Knacke, O. Kubaschewski, K. Hesselmann (Eds.), Thermochemical Properties of Inorganic Substances, 2nd ed., Springer-Verlag, New York, 1991, pp. 1455–1456.

[27] C.Y. Chen, T.K. Tseng, S.C. Tsai, C.K. Lin, H.M. Lin, Effect of precursor characteristics on zirconia and ceria particle morphology in spray pyrolysis, Ceram. Int. 34 (2008) 409–416.
[28] C.Y. Chen, W.H. Tuan, Effect of silver on the sintering and grain-growth behavior of barium titanate, J. Am. Ceram. Soc. 83 (2000) 2988–2992.
[29] B.G. Pound, The characterization of doped CeO_2 electrodes in solid oxide fuel cells, Solid State Ionics 52 (1992) 183–188.
[30] J. Ranløv, F.W. Poulsen, M. Mogensen, Comment on "The characterization of doped CeO_2 electrodes in solid oxide fuel cells" by B.G. Pound, Solid State Ionics, 52 (1992), 183–188, Solid State Ionics 61 (1993) 277–279.
[31] P. Datta, P. Majewski, F. Aldinger, Synthesis and reactivity study of gadolinia doped ceria–nickel: a potential anode material for solid oxide fuel cell, J. Alloys Compd. 455 (2008) 454–460.
[32] Y.S. Zhen, S.J. Milne, R.J. Brook, Oxygen ion conduction in CeO_2 ceramics simultaneously doped with Gd_2O_3 and Y_2O_3, Sci. Ceram. 14 (1988) 1025–1030.
[33] J.-F. Fue, J. Jusko, A.V. Virkar, Electrochemical vapor deposition of cerium dioxide: kinetics of deposition of a composite, two-layer electrolyte, J. Electrochem. Soc. 139 (1992) 2458–2461.
[34] W. Zając, J. Molenda, Electrical conductivity of doubly doped ceria, Solid State Ionics 179 (2008) 154–158.
[35] P. Muralidharan, S.H. Jo, D.K. Kim, Electrical conductivity of submicrometer gadolinia-doped ceria sintered at 1000 °C using precipitation-synthesized nanocrystalline powders, J. Am. Ceram. Soc. 91 (2008) 3267–3274.
[36] H. Xu, H. Yan, Z. Chen, Preparation and properties of Y^{3+} and Ca^{2+} co-doped ceria electrolyte materials for ITSOFC, Solid State Sci. 10 (2008) 1179–1184.
[37] M. Mogensena, N.M. Sammes, G.A. Tompsett, Physical, chemical and electrochemical properties of pure and doped ceria, Solid State Ionics 129 (2000) 63–94.